PONTRYAGIN APPROXIMATIONS FOR OPTIMAL DESIGN OF ELASTIC STRUCTURES

JESPER CARLSSON

Abstract. This article presents a numerical method for approximation of some optimal control problems for partial differential equations. The method uses regularization derived from consistency with the corresponding Hamilton-Jacobi-Bellman equations in infinite dimension. In particular, optimal designs of elastic structures such as distributing a limited amount of material to minimize its compliance, or to detect interior material distributions from surface measurements, are computed. The derived Pontryagin based method presented here is simple to use with standard PDE-software using Newton iterations with a sparse Hessian.

Contents

1. The Optimal Design Problem

Optimal design can be described as the particular inverse problem of controlling a partial differential equation to meet some design criteria in an optimal way. The control typically consists of changing the computational domain (shape optimization) or distributing a coefficient in the partial differential equation (parameter design). It is well known that these inverse problems often are ill posed, *e.g.* small perturbations of data lead to large changes in the solution, and need to be regularized to obtain good approximations, *cf.* [6, 13]. The goal of this article is to investigate a numerical method, based on a regularization derived from consistency with the corresponding Hamilton-Jacobi-Bellman equation in infinite dimension, for the particular problem of optimally controlling the partial differential equations of linear elasticity. This extends the work in [11], for control of ordinary differential equations, and [3], for control of scalar partial differential equations.

This article focuses on two types of inverse problems in elasticity: to optimally design an elastic structure and to optimally reconstruct an unknown elastic structure from boundary measurements. The first is a typical problem in optimal design where the objective is to place a given amount of elastic material, submitted to

2000 *Mathematics Subject Classification.* Primary: 65N21; Secondary: 49L25.

Key words and phrases. Topology Optimization, Inverse Problems, Hamilton-Jacobi, Regularization.

Support by the Swedish Research Council grants 2002-6285 and 2002-4961, and the European network HYKE, funded by the EC as contract HPRN-CT-2002-00282, is acknowledged.

static equilibrium and prescribed volume and surface forces, in a given domain $\Omega \in \mathbb{R}^d$, in order to maximize its stiffness. An alternative similar problem is to minimize the compliance

$$l(u) \equiv \int_\Omega f_b \cdot u \, \mathrm{d}x + \int_{\Gamma_N} f_s \cdot u \, \mathrm{d}s, \tag{1}$$

where $u : \Omega \to \mathbb{R}^d$ denotes the displacements at static equilibrium when applying given volume forces $f_b : \Omega \to \mathbb{R}^d$ and surface forces $f_s : \Gamma_N \to \mathbb{R}^d$, $\Gamma_N \subset \partial\Omega$. For convenience it is here assumed that a part of the boundary is fixed, *i.e.* $u_{\Gamma_D} = 0$ where $\Gamma_D = \partial\Omega \setminus \Gamma_N \neq \emptyset$.

For a linearly elastic material, the work done by a virtual displacement v at static equilibrium, can described by the bilinear energy functional

$$a_\rho(u, v) \equiv \int_\Omega \rho \varepsilon_{ij}(u) E_{ijkl} \varepsilon_{kl}(v) \, \mathrm{d}x, \quad i, j, k, l = 1, \ldots, d, \tag{2}$$

with a relative material density ρ, linearized strains $\varepsilon_{ij}(u) = \frac{1}{2}(\frac{\partial u_i}{\partial x_j} + \frac{\partial u_j}{\partial x_i})$ and an elasticity tensor E_{ijkl}. We here use the Einstein summation convention for summation over indices occurring more than once in an expression. The elasticity tensor relates linearized strains to linearized stresses by Hooke's law $\sigma_{ij} = E_{ijkl}\varepsilon_{kl}$, which for an isotropic material can be written as

$$\sigma_{ij} = \lambda \delta_{ij} \varepsilon_{kk} + 2\mu \varepsilon_{ij} \tag{3}$$

where λ and μ are the Lamé coefficients, and δ_{ij} denote the Kronecker delta. From the principle of virtual work, the displacement $u \in V = \{v \in H^1(\Omega)^d | v_{\Gamma_D} = 0\}$ at equilibrium, must then satisfy the variational equation

$$a_\rho(u, v) = l(v), \quad \forall v \in V. \tag{4}$$

To indicate void or material an ideal relative material density would be to let $\rho : \Omega \to \{0, 1\}$, but in order for (4) to be well defined we restrict the density to $\rho : \Omega \to \{\rho_-, 1\}$ with some small $\rho_- > 0$.

In summary, the problem to optimally design a structure with minimal compliance, for some fixed volume C, can be formulated as the minimization problem

$$\inf_{\rho:\Omega\to\{\rho_-,1\}} \left\{ l(u) \;\middle|\; a_\rho(u, v) = l(v), \ \forall v \in V, \ \int_\Omega \rho \, \mathrm{d}x = C \right\}. \tag{5}$$

Since the volume constraint in (5) is difficult to handle, we here use an alternative formulation, were the volume constraint is relaxed by introducing a corresponding Lagrange multiplier $\eta \in \mathbb{R}$. This gives the simpler problem

$$\inf_{\rho:\Omega\to\{\rho_-,1\}} \left\{ l(u) + \eta \int_\Omega \rho \, \mathrm{d}x \;\middle|\; a_\rho(u, v) = l(v), \ \forall v \in V \right\}. \tag{6}$$

In a real application, η of course needs to be determined to meet the desired volume C, but as a preliminary step we consider (6) with some a priori value of η. In practice, the multiplier could be determined by solving (6) in an inner loop and iteratively changing η in an outer loop, but to come up with an effective procedure for this is a difficult task not dealt with here. Observe that (5) and (6) are not truly equivalent, since even though every choice of volume in (5) corresponds to a unique multiplier η, the converse is not necessarily true.

It is well known that (5) and (6) are ill-posed minimization problems in the sense that existence of a minimizer cannot be guaranteed [1]. In fact, a minimizing sequence $\{\rho_n\}$ would oscillate more wildly as $n \to \infty$ and the limit would not even belong to the discrete set $\{\rho_-, 1\}$ anymore. The general cure of ill-posedness of this optimal design problem is to introduce a proper relaxation of the set of admissible designs, thus replacing (6) with a well-posed problem. This can be done by adding

a penalty on the variation of the control ρ, so called Tikhonov regularization, or in this particular case by allowing intermediate densities $\rho : \Omega \to [\rho_-, 1]$, the so called plate thickness problem [2]. Another approach is to minimize (6) over the class $\mathcal{E}_\mathcal{C}$ of elasticity tensors for certain composites of materials, *i.e.*

$$\min_{\rho\in[\rho_-,1],E\in\mathcal{E}_\mathcal{C}} \left\{ l(u) + \eta \int_\Omega \rho \, \mathrm{d}x \;\middle|\; a_{\rho,E}(u,v) = l(v),\ \forall v \in V \right\}, \tag{7}$$

where $a_{\rho,E}(u,v) \equiv a_\rho(u,v)$ to indicate the dependence of E. Here, the tensor E now describes the micro-structure of the material, and for the right choice of $\mathcal{E}_\mathcal{C}$, *e.g.* sequential laminated composites, the minimization problem (7) is well posed, and the solution corresponds to a homogenized optimal design, *cf.* [1]. Homogenization in optimal design is closely connected to the concept of quasi-convexity, which in the standard theory of variational calculus is a necessary condition for the existence of a minimizer [5]. In fact, homogenization or quasi-convexification gives truly optimal designs in the sense that the minimum of (7) coincides with the infimum of (6). Ill-posed problems related to optimal design has been studied extensively in the context of relaxation by quasi-convexification and homogenization in for example [1, 7, 8] and [9].

In Section 2, we derive an alternative regularization which can be compared to a Tikhonov type penalty. The regularization is based on the Hamilton-Jacobi-Bellman equation corresponding to the optimal control problem (6) and the existence of a minimizer essentially depends on the quasi-convexity of the Hamiltonian. Numerical examples for the particular problem (6) are studied in Section 4.

Another inverse problem studied in Section 4 is the reconstruction of an unknown density from boundary measurements: apply given forces $f_s : \Gamma_N \to \mathbb{R}^d$ and reconstruct the interior density $\rho : \Omega \to \{\rho_-, 1\}$ from the resulting boundary displacements u_{meas} on Γ_N by minimizing

$$\inf_{\rho:\Omega\to\{\rho_-,1\}} \left\{ \int_{\Gamma_N} |u - u_{meas}|^2 \, \mathrm{d}s \;\middle|\; a_\rho(u,v) = l(v),\ \forall v \in V \right\}. \tag{8}$$

The problem to determine ρ is in general ill-posed due to non-continuous dependence on measured data. For this problem Tikhonov type regularization methods therefore seem standard, since to introduce intermediate values $\rho : \Omega \to [\rho-, 1]$ is not sufficient. Note, that the measurements u_{meas} may be restricted to a subset of Γ_N and can also be contaminated by noise, which makes (8) even harder to solve without proper regularization. Also note that the above optimal control problems (6) and (8) are single-load problems which easily can be extended to the multi-load case. In Section 4 we present some numerical results for the reconstruction problem (8) using multiple loads.

2. Pontryagin Approximations for Optimal Control

It is well known that inverse problems need to be regularized to obtain good approximations [6], and regularization may also be necessary to assure the mere existence of a solution. In the following section we present a Pontryagin method for optimal control of partial differential equations using a regularization derived from consistency with the corresponding Hamilton-Jacobi-Bellman equations in infinite dimension. To make the presentation clear and concise we first describe the method for controlling a system of ordinary differential equations, and then apply the methodology to control of partial differential equations, following [3].

Consider the optimal control problem for a controlled ordinary differential equation

$$\inf_{\alpha\in\mathcal{A}} \left\{ g(X(T)) + \int_0^T h(X(s),\alpha(s)) \, \mathrm{d}s \;\middle|\; X'(t) = f(X(t),\alpha(t)),\ X(0) = X_0 \right\}, \tag{9}$$

with given data $g : \mathbb{R}^n \to \mathbb{R}$, $h : \mathbb{R}^n \times B \to \mathbb{R}$, $f : \mathbb{R}^n \times B \to \mathbb{R}^n$, $X_0 \in \mathbb{R}^n$, the state variable $X : [0,T] \to \mathbb{R}^n$ and a set of controls $\mathcal{A} = \{\alpha : [0,T] \to B \subset \mathbb{R}^m\}$. Optimal control problems like (9) can be solved by dynamic programming or by the Lagrange principle. Defining the value function

$$u(x,t) \equiv \inf_{X(t)=x, \alpha \in \mathcal{A}} \left\{ g\big(X(T)\big) + \int_t^T h\big(X(s), \alpha(s)\big) \ \mathrm{d}s \right\},$$

the dynamic programming approach gives that $u : \mathbb{R}^n \times [0,T] \to \mathbb{R}$ is the bounded uniformly continuous viscosity solution of the nonlinear Hamilton-Jacobi-Bellman partial differential equation

$$\begin{aligned} \partial_t u(x,t) + H\big(\partial_x u(x,t), x\big) = 0, \qquad & (x,t) \in \mathbb{R}^n \times (0,T), \\ u(x,T) = g(x), \qquad & x \in \mathbb{R}^n, \end{aligned} \tag{10}$$

where the Hamiltonian function $H : \mathbb{R}^n \times \mathbb{R}^n \to \mathbb{R}$ is defined by

$$H(\lambda, x) \equiv \min_{\alpha \in B} \big\{ \lambda \cdot f(x,\alpha) + h(x,\alpha) \big\}.$$

The Hamilton-Jacobi partial differential equation approach has the advantage that a global minimum is found, but cannot be used computationally for high dimensional problems where $n \gg 1$, and gives no direct information on the optimal path $X(t)$ and control $\alpha(t)$. On the other hand, assuming that H, f, g, h are differentiable, the Lagrange principle gives that an optimal path $X(t)$ satisfies the Hamiltonian boundary value system

$$\begin{aligned} X'(t) &= \partial_\lambda H\big(\lambda(t), X(t)\big), \quad X(0) = X_0, \\ -\lambda'(t) &= \partial_x H\big(\lambda(t), X(t)\big), \quad \lambda(T) = g'(X(T)), \end{aligned} \tag{11}$$

Solving (11) is actually the method of characteristics for the Hamilton-Jacobi equation (10) provided $\lambda(t) \equiv \partial_x u(X(t), t)$ exists. Also note that equation (11) is equal to

$$\begin{aligned} X'(t) &= f\big(X(t), \alpha(t)\big), \\ X(0) &= X_0, \\ -\lambda_i'(t) &= \partial_{x_i} f\big(X(t), \alpha(t)\big) \cdot \lambda(t) + h_{x_i}\big(X(t), \alpha(t)\big), \\ \lambda(T) &= g'\big(X(T)\big). \end{aligned}$$

with the control α determined by the Pontryagin principle

$$\alpha(t) \in \mathrm{argmin}_{a \in B} \ \big\{ \lambda(t) \cdot f(X(t), a) + h(X(t), a) \big\}, \tag{12}$$

The Lagrange principle has the advantage that high dimensional problems, $n \gg 1$ can be solved computationally and the drawback is that in practice only local minima can be found computationally. Also, when using (11) to solve the minimization problem (9) it is assumed that the Hamiltonian is explicitly known and differentiable. In general, Hamiltonians are only Lipschitz continuous for smooth f, g and h. As we will see in Section 4, explicit Hamiltonians do exist for many interesting applications, and they can be approximated by differentiable ones. To emphasize the connection with the optimal control we refer to solving (11) as the *Pontryagin method*.

Many optimal control problems lead to non-smooth optimal controls, *e.g.* bang-bang controls, which occur by two reasons: the Hamiltonian is in general only Lipschitz continuous, even though f, g, h are smooth, and backward optimal paths $X(t)$ may collide. The theory of viscosity solutions to Hamilton-Jacobi equations elegantly handles non-smooth solutions, but to be able to use the computational advantage of solving the Hamiltonian boundary value system (11) we introduce a regularized problem with a $\mathcal{C}^2(\mathbb{R}^n \times \mathbb{R}^n)$ λ-concave approximation H_δ of the

Hamiltonian H. This approximation not only gives meaning to (11), but is well defined in the sense that the corresponding approximated value function u_δ is close to the original value function u. In [11], error analysis yields the estimate

$$\|u_\delta - u\|_{L^\infty(\mathbb{R}^d \times \mathbb{R}_+)} = \mathcal{O}(\delta), \tag{13}$$

for the real and approximate value functions u and u_δ, and with a regularization parameter δ, such that $\|H_\delta - H\|_{L^\infty(\mathbb{R}^n \times \mathbb{R}^n)} = \mathcal{O}(\delta)$. This error estimate is not explicitly dependent on the dimension n and is thus suitable for optimal control of discretized partial differential equations. Observe that $\|u_\delta - u\|_{L^\infty(\mathbb{R}^n \times \mathbb{R}_+)} \to 0$ does not necessarily imply convergence of the optimal paths $X(t)$ or the controls $\alpha(t)$.

Now, consider the above analysis extended to control of a time dependent partial differential equation, as in [3],

$$\begin{aligned} \partial_t \varphi(x,t) &= f\big(\varphi(x,t), \alpha(x,t)\big), \quad (x,t) \in \Omega \times (0,T) \\ \varphi(x,0) &= \varphi_0, \qquad\qquad\qquad\quad x \in \Omega \end{aligned}$$

where f is a partial differential operator, $\Omega \subset \mathbb{R}^n$, and $\varphi(\cdot,t)$ belongs to some Hilbert space V on Ω. The minimization problem corresponding to (9) then becomes

$$\inf_{\alpha:\Omega\times[0,T]\to B} \left\{ g\big(\varphi(\cdot,T)\big) + \int_0^T h\big(\varphi(\cdot,t), \alpha(\cdot,t)\big)\ \mathrm{d}t \;\middle|\; \partial_t \varphi = f\big(\varphi(\cdot,t), \alpha(\cdot,t)\big),\ \varphi(\cdot,0) = \varphi_0 \right\}, \tag{14}$$

The Hamiltonian $H : V \times V \to \mathbb{R}$ is defined as

$$H(\lambda, \varphi) \equiv \min_{\alpha:\Omega\to B} \{\langle \lambda, f(\varphi,\alpha)\rangle + h(\varphi,\alpha)\}, \tag{15}$$

and the value function $u : V \times [0,T] \to \mathbb{R}$,

$$u(\phi,\tau) \equiv \inf_{\alpha:\Omega\times[0,T]\to B} \left\{ g\big(\varphi(\cdot,T)\big) + \int_\tau^T h\big(\varphi(\cdot,t), \alpha(\cdot,t)\big)\ \mathrm{d}t \;\middle|\; \partial_t \varphi = f\big(\varphi(\cdot,t), \alpha(\cdot,t)\big),\ \varphi(\cdot,\tau) = \phi \in V \right\}$$

solves the Hamilton-Jacobi-Bellman equation

$$\partial_t u(\phi,t) + H\big(\partial_\phi u(\phi,t), \phi\big) = 0, \quad u(\cdot,T) = g. \tag{16}$$

Here, ∂ now denotes Gâteaux derivatives (except for ∂_t), and $\langle v, w\rangle$ is the duality pairing on V, which reduces to the $L^2(\Omega)$ inner product if $v, w \in L^2(\Omega)$. From the Lagrange principle we get the Hamiltonian system

$$\begin{aligned} \partial_t \varphi &= \partial_\lambda H(\lambda,\varphi), \qquad \varphi(\cdot,0) = \phi \\ \partial_t \lambda &= -\partial_\varphi H(\lambda,\varphi), \quad \lambda(\cdot,T) = \partial_\varphi g\big(\varphi(\cdot,T)\big). \end{aligned} \tag{17}$$

To solve (17), consider a finite element subspace $\bar{V} \subset V$ and a corresponding $\mathcal{C}^2$ regularized approximate Hamiltonian $\bar{H}_\delta : V \times \bar{V} \to \mathbb{R}$,

$$\bar{H}_\delta(\lambda,\bar{\varphi}) \equiv \min_{\alpha:\Omega\to B} \{\langle \lambda, f_\delta(\bar{\varphi},\alpha)\rangle + h_\delta(\bar{\varphi},\alpha)\},$$

with approximations f_δ and h_δ. For $\varphi, \lambda \in \bar{V}$, the problem has now been transformed into the control of a system of ordinary differential equations, so the estimate (13) still holds for the value functions $\bar{u}_\delta$ and $\bar{u}$ solving (16) using $\bar{H}_\delta$ and the unregularized Hamiltonian $\bar{H} : V \times \bar{V} \to \mathbb{R}$ respectively, see [3, 11]. An error estimate for the difference between the true value function u and the regularized approximate value function $\bar{u}_\delta$ is however harder to derive, since it seems to require knowledge of the difference between true optimal paths (φ, λ) and approximated

optimal paths $(\bar{\varphi}_\delta, \bar{\lambda}_\delta)$. As noted earlier these paths does in general not converge for a non-differentiable Hamiltonian, since the control becomes discontinuous. In [3], an estimate of $u - \bar{u}_\delta$, using only the difference of H and $\bar{H}_\delta$ along the same path, is derived. This estimate gives an error estimate which in practice can be bounded in terms of the regularization parameter δ and the finite element mesh size, such that the value functions converge even though the optimal paths do not. For more on this issue, see [3, 12].

In the following sections the Pontryagin method is used for solving time independent optimal design problems with only Lipschitz continuous Hamiltonians. All examples presented give Lipschitz continuous Hamiltonians which need to be regularized.

3. Concave Maximization

To apply the methodology of time dependent optimal control from Section 2 to the time independent optimal design problem in Section 1, we first concentrate on a simpler scalar problem of electric conductivity [10]: to place a given amount of conducting material in a given domain $\Omega \subset \mathbb{R}^d$ in order to minimize the power loss for a given surface current q, satisfying $\int_{\partial\Omega} q \, \mathrm{d}s = 0$. Let, as in Section 1, $\eta \in \mathbb{R}$ be a given constant, associated to the given amount of material, and find an optimal conduction distribution $\sigma : \Omega \to \{\sigma_-, \sigma_+\}$, where $\sigma_\pm > 0$, such that

$$\inf_\sigma \left\{ \int_{\partial\Omega} q\varphi \;\; \mathrm{d}s + \eta \int_\Omega \sigma \;\; \mathrm{d}x \;\middle|\; \operatorname{div}(\sigma\nabla\varphi)\big|_\Omega = 0, \;\; \sigma\frac{\partial\varphi}{\partial n}\Big|_{\partial\Omega} = q \right\}, \tag{18}$$

here $\partial/\partial n$ denotes the normal derivative, $\mathrm{d}s$ is the surface measure on $\partial\Omega$ and $\varphi \in V \equiv \{v \in H^1(\Omega) : \int_\Omega v \, \mathrm{d}x = 0\}$ is the electric potential.

Now, consider the parabolic variant of the constraint in (18), with $\sigma : \Omega \times [0,T] \to \{\sigma_-, \sigma_+\}$, $\varphi : \Omega \times [0,T] \to \mathbb{R}$ and initial data $\varphi_0 \in V$:

$$\begin{aligned} \partial_t\varphi &= \operatorname{div}\big(\sigma\nabla\varphi\big), && (x,t) \in \Omega \times (0,T) \\ \sigma\frac{\partial\varphi}{\partial n} &= q(x), && (x,t) \in \partial\Omega \times (0,T) \\ \varphi(x,0) &= \varphi_0, && x \in \Omega, \end{aligned}$$

and the time dependent minimization problem

$$\begin{aligned} \inf_\sigma \Bigg\{ \int_0^T \int_{\partial\Omega} q\varphi \;\; \mathrm{d}s + \eta \int_\Omega \sigma \;\; \mathrm{d}x \;\; \mathrm{d}t \;\Bigg| \\ \partial_t\varphi = \operatorname{div}(\sigma\nabla\varphi), \;\; \sigma\frac{\partial\varphi}{\partial n}\Big|_{\partial\Omega} = q, \;\; \varphi(\cdot,0) = \varphi_0 \Bigg\}. \end{aligned} \tag{19}$$

The Lagrangian takes the form

$$\mathcal{L}(\sigma,\lambda,\varphi) := \int_0^T \int_{\partial\Omega} q(\varphi+\lambda) \;\; \mathrm{d}s \;\; \mathrm{d}t + \int_0^T \int_\Omega \sigma \underbrace{(\eta - \nabla\varphi\cdot\nabla\lambda)}_{\mathfrak{v}} - \partial_t\varphi\lambda \;\; \mathrm{d}x \;\; \mathrm{d}t,$$

with $\lambda = \lambda(x,t)$ and the Hamiltonian corresponding to (15) becomes

$$\begin{aligned} H(\lambda,\varphi) &= \min_{\sigma:\Omega\to\{\sigma_\pm\}} \left\{ \int_\Omega \sigma\mathfrak{v} \;\; \mathrm{d}x + \int_{\partial\Omega} q(\varphi+\lambda) \;\; \mathrm{d}s \right\} \\ &= \int_\Omega \underbrace{\min_{\sigma\in\{\sigma_-,\sigma_+\}} \{\sigma\mathfrak{v}\}}_{\mathfrak{h}(\mathfrak{v})} \;\; \mathrm{d}x + \int_{\partial\Omega} q(\varphi+\lambda) \;\; \mathrm{d}s. \end{aligned} \tag{20}$$

As in Section 2, the value function

$$u(\phi,\tau)=\inf_{\sigma}\left\{\int_\tau^T\int_{\partial\Omega} q\varphi\ \ \mathrm{d}s+\eta\int_\Omega\sigma\ \ \mathrm{d}x\ \ \mathrm{d}t\ \middle|\ \partial_t\varphi=\operatorname{div}(\sigma\nabla\varphi),\ \sigma\frac{\partial\varphi}{\partial n}\Big|_{\partial\Omega}=q,\ \varphi_\tau=\phi\right\}$$

satisfies the infinite dimensional Hamilton-Jacobi equation

$$\partial_t u(\phi,t)+H(\partial_\phi u(\phi,t),\phi)=0\quad t<T,\quad u(\cdot,T)=0,$$

using the Gâteaux derivative $\partial_\phi u(\phi,t)$ of the functional $u(\phi,t)$ in $L^2(\Omega)$. The corresponding Hamiltonian system is the parabolic system

$$\begin{aligned}\int_\Omega \partial_t\varphi w+\mathfrak{h}'(\eta-\nabla\varphi\cdot\nabla\lambda)\nabla\varphi\cdot\nabla w\ \ \mathrm{d}x&=\int_{\partial\Omega} qw\ \ \mathrm{d}s,\quad \varphi(\cdot,0)=\varphi_0,\\ \int_\Omega -\partial_t\lambda v+\mathfrak{h}'(\eta-\nabla\varphi\cdot\nabla\lambda)\nabla\lambda\cdot\nabla v\ \ \mathrm{d}x&=\int_{\partial\Omega} qv\ \ \mathrm{d}s,\quad \lambda(\cdot,T)=0,\end{aligned}\tag{21}$$

for all test functions $v,w\in V\equiv\{v\in H^1(\Omega):\int_\Omega v\ \ \mathrm{d}x=0\}$.

From (20) it is evident that the control becomes undefined and the Hamiltonian non-differentiable when $\mathfrak{v}\equiv\eta-\nabla\varphi\cdot\nabla\lambda=0$. We thus replace H with the concave regularization H_δ depending on a smooth approximation, $\mathfrak{h}_\delta\in\mathcal{C}^2(\mathbb{R})$, of the Lipschitz continuous and monotonically increasing function $\mathfrak{h}$, see left part of Figure 1. In this case the regularization H^δ is therefore similar to a Tikhonov reg-

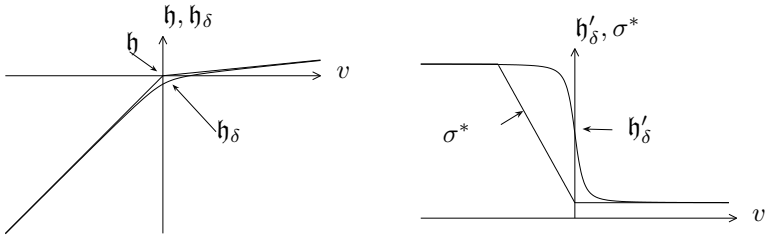

FIGURE 1. Left: The function $\mathfrak{h}$ and its regularization $\mathfrak{h}_\delta$ with respect to $\mathfrak{v}$. Right: The approximation $\mathfrak{h}'_\delta$ compared to a control σ^* obtained from adding a Tikhonov type penalty $\delta\int_\Omega\sigma^2\ \mathrm{d}x$ to (20) with $\sigma:\Omega\to[\sigma_-,\sigma_+]$.

ularization with penalty on the L^2 norm of σ, see right part of Figure 1. Note that $\sigma:\Omega\to[\sigma_-,\sigma_+]$ in (20) will lead to the same Hamiltonian as $\sigma:\Omega\to\{\sigma_-,\sigma_+\}$.

To connect the optimal design problem (18) with the artificial time-dependent problem (19) we assume that

$$\lim_{T\to\infty}\frac{u(\cdot,0)}{T}=\inf_\sigma\left\{\int_{\partial\Omega} q\varphi\ \ \mathrm{d}s+\eta\int_\Omega\sigma\ \ \mathrm{d}x\ \middle|\ \operatorname{div}(\sigma\nabla\varphi)\Big|_\Omega=0,\ \sigma\frac{\partial\varphi}{\partial n}\Big|_{\partial\Omega}=q\right\},$$

which can be achieved by assuming $\partial_t\varphi=\partial_t\lambda=0$ in the Hamiltonian system (21). Time independent solutions to (21) exhibits symmetry $\varphi=\lambda$ and solves the nonlinear elliptic partial differential equation

$$\begin{aligned}\operatorname{div}\big(\mathfrak{h}'_\delta(\eta-|\nabla\varphi|^2)\nabla\varphi\big)&=0,\quad x\in\Omega\\ \mathfrak{h}'_\delta\frac{\partial\varphi}{\partial n}&=q,\quad x\in\partial\Omega\end{aligned}\tag{22}$$

which can be formulated as the concave maximization problem: $\varphi \in V$ is the unique maximizer of

$$H_\delta(\varphi,\varphi) = \int_\Omega \mathfrak{h}_\delta(\eta - |\nabla\varphi(x)|^2)\ \mathrm{d}x + 2\int_{\partial\Omega} q\varphi\ \mathrm{d}s.$$

An advantage with the Pontryagin approach (22) is that the Hessian of H_δ can be determined explicitly and is sparse, so that the Newton method can be used for iterative solution of (22). Note that the opposite problem of maximizing power loss, *i.e.* replacing the 'inf' in (18) with a 'sup', would in general not give a concave regularized Hamiltonian H_δ. The existence of a maximizer φ depends on the weak upper semi-continuity of H_δ, which in this particular case can be guaranteed if $\mathfrak{h}_\delta$ is concave with respect to $|\nabla\varphi|$, see [5]. In Figure 2, $\mathfrak{h}$ and $\mathfrak{h}_\delta$ are shown as functions of $|\nabla\varphi|$ for both minimizing and maximizing power loss. The function $\mathfrak{h}_\delta$ for the problem of maximizing power loss is only concave for sufficiently large regularizations.

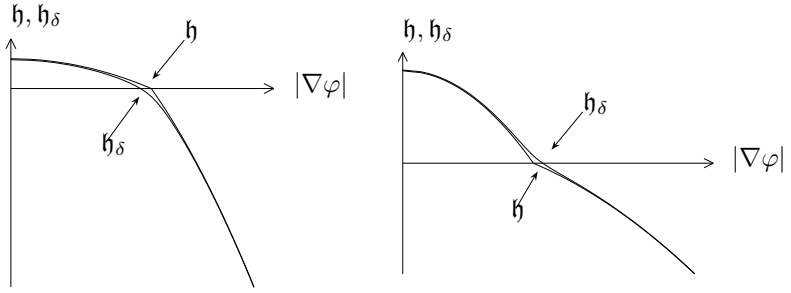

FIGURE 2. The function $\mathfrak{h}$ and its regularization $\mathfrak{h}_\delta$ with respect to $|\nabla\varphi|$ when minimizing power loss (left) and maximizing power loss (right).

4. Numerical Examples

To numerically solve the optimal design problems (6) and (8) in Section 1, we consider the planar stress case, $\sigma_{3l} = \sigma_{l3} = 0$, $l = 1, 2, 3$, for a thin plate located in the xy-plane. The plate can be described by the two dimensional domain $\Omega \subset \mathbb{R}^2$, and the material density ρ can be interpreted as the thickness of the plate. For planar forces $f_b : \Omega \to \mathbb{R}^2$ and $f_s : \Gamma_N \to \mathbb{R}^2$, $\Gamma_N \subset \partial\Omega$, the planar displacements $u : \Omega \to \mathbb{R}^2$ can be separated from the anti-planar displacement, and satisfy the variational equation (4), for $d = 2$. The Lamé coefficients in Hooke's law (3) takes the form

$$\mu = \frac{E}{2(1+\nu)}, \quad \lambda = \frac{E\nu}{1-\nu^2},$$

with a Young's modulus E and a Poisson ratio ν. In all examples we assume $E = 100$, $\nu = 0.3$, and that no volume forces are present, *i.e.* $f_b = 0$.

4.1. **Compliance Optimization.** Recall the compliance minimization problem (6), *i.e.*

$$\inf_\rho \left\{ l(u) + \eta \int_\Omega \rho\ \mathrm{d}x \;\middle|\; a_\rho(u,v) = l(v),\ \forall v \in V \right\}.$$

with relative material density $\rho : \Omega \to \{\rho_-, 1\}$, displacement $u : \Omega \to \mathbb{R}^2$, compliance functional $l(u)$ and bilinear energy functional $a_\rho(u,v)$. Similarly to Section 3,

we note that the Lagrangian takes the form

$$\mathcal{L}(u,\lambda,\rho) = l(u) + l(\lambda) + \int_\Omega \rho \underbrace{\left(\eta - \sum_{ijkl} \varepsilon_{ij}(u) E_{ijkl} \varepsilon_{kl}(\lambda) \right)}_{\mathfrak{v}} \, \mathrm{d}x,$$

and the Hamiltonian is

$$H(u,\lambda) = l(u) + l(\lambda) + \int_\Omega \underbrace{\min_{\rho \in \{\rho_-, 1\}} \{\rho \mathfrak{v}\}}_{\mathfrak{h}(\mathfrak{v})} \, \mathrm{d}x.$$

Regularizing $\mathfrak{h}$ with $\mathfrak{h}_\delta$, and consequently H with H^δ, gives a Hamiltonian system which by symmetry, $u = \lambda$, can be reduced to the variational equation

$$\int_\Omega \mathfrak{h}'_\delta \left(\eta - \sum_{mnop} \varepsilon_{mn}(u) E_{mnop} \varepsilon_{op}(u) \right) \varepsilon_{ij}(u) E_{ijkl} \varepsilon_{kl}(v) \, \mathrm{d}x = l(v) \tag{23}$$

for all admissible displacements $v \in V = \{H^1(\Omega)^d, v_{\Gamma_D} = 0\}$, which is the Euler-Lagrange equation of the problem to find the unique maximizer $u \in V$ of the functional

$$H^\delta = 2l(u) + \int_\Omega \mathfrak{h}_\delta \left(\eta - \sum_{ijkl} \varepsilon_{ij}(u) E_{ijkl} \varepsilon_{kl}(u) \right) \, \mathrm{d}x. \tag{24}$$

In all numerical tests for the compliance minimization problem we let Ω be the rectangular domain defined by $(x, y) \in (0, 2) \times (0, 1)$, and solve (23) on the finite element subspace consisting of nine-node quadrilateral elements on a uniform mesh. The left boundary is fixed and a downward force, $f_s(2, y) = -10$, $y \in [0.45, 55]$, is applied to the middle of the right boundary. The lower bound on the material density is $\rho_- = 10^{-3}$, and the regularized function $\mathfrak{h}_\delta$ is chosen such that

$$\mathfrak{h}'_\delta(\mathfrak{v}) = \frac{1}{2} \left(\rho_- + 1 + (\rho_- - 1) \tanh \left(\frac{\mathfrak{v} \ \tanh^{-1}(0.99)}{\delta} \right) \right),$$

see Figure 1. The resulting discrete system is solved with Newton's method and for successively smaller regularizations according to the scheme:

- if the Newton method for δ_{old} converged choose

$$\delta_{new} = \alpha_{old} \delta_{old}, \quad \alpha_{new} = \alpha_{old},$$

- otherwise let

$$\delta_{new} = \frac{1}{2} \delta_{old} (1 + \frac{1}{\alpha_{old}}), \quad \alpha_{new} = \frac{2\alpha_{old}}{\alpha_{old} + 1}.$$

This means that if the Newton method fails to converge for some regularization δ, the new regularization will be the average of δ and the last successful regularization. Also, the parameter α is constructed such that if this new averaged regularization works, we will once again try the regularization where the method previously failed. Here, $\alpha_{old} = 0.5$ is used as initial step-size.

In the left part of Figure 3 to Figure 7, the variational equation (23) is solved using FEMLAB and the Newton method for successively smaller values of δ. As δ is reduced the density will not achieve purely discrete values, but rather remain at intermediate values in large regions. This agrees with results from other regularizations, such as the plate thickness approach [2] or the homogenization method [1]. The smooth density is consistent with the fact that a minimizing sequence for the original formulation (6) will oscillate in these areas, and the regularized solution will behave approximately as an average of these oscillations.

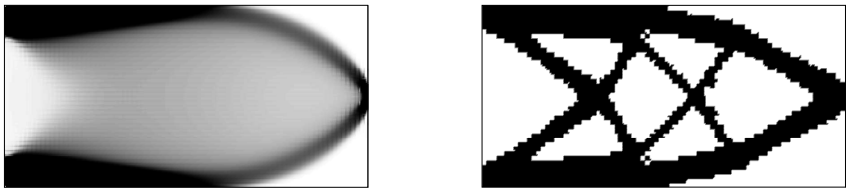

FIGURE 3. Plot of $\mathfrak{h}'_\delta$ as an approximation of the relative material density when minimizing compliance of an elastic plate with a fixed right side and an external load $f_s(2, y) = -10$, $y \in [0.45, 55]$. A uniform mesh with 80×40 nine-node quadrilateral finite elements and a multiplier $\eta = 5 \cdot 10^{-3}$ was used. In the left figure, (4) was solved with the Newton method and by successively reducing the regularization δ until $\delta \approx 3.5 \cdot 10^{-4}$. The right figure shows the density after 100 iterations using (25) with $\delta = 0$ and with the solution from the left part taken as initial guess.

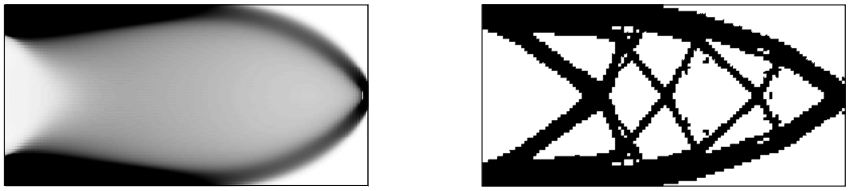

FIGURE 4. Plot of $\mathfrak{h}'_\delta$ calculated with data as in Figure 3 but using a 240×120 mesh. Note that the unregularized design on the right is mesh dependent. The discrete designs are also sensitive to the initial data and the fraction of elements allowed to change in each iteration. Although the discrete design here differs a lot from the one in Figure 3, the compliance only differs by less than 0.1 percent.

Since ρ can be determined explicitly by the Pontryagin method an alternative approach to solving (23) with the Newton method is to iterate separately over ρ and u according to the scheme

$$\rho_{m+1} = \mathfrak{h}'_\delta\Big(\eta - \sum_{ijkl} \varepsilon_{ij}(u_m) E_{ijkl} \varepsilon_{kl}(u_m)\Big) \tag{25}$$

where u_m solves (23) with $\rho = \rho_m$. This scheme, which essentially is the Jacobi method, is highly unstable since information from the Hessian is lost. It is, however, still possible to use this method, with $\delta = 0$, as post-processing to eliminate areas of intermediate density generated by the Newton method. In general, such discrete

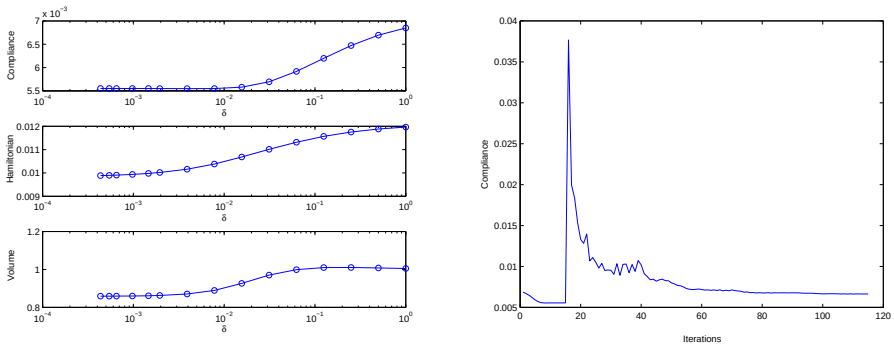

FIGURE 5. Convergence plots corresponding to Figure 4. Left: Convergence of the compliance, the Hamiltonian, and the volume with respect to the regularization. Right: Plot of the compliance for the discrete iterations corresponding to the right plot in Figure 4. The values from the left plot is included in the first iterations for comparison. Note that although the compliance for the discrete iterations decreases it will never reach the compliance for the regularized problem.

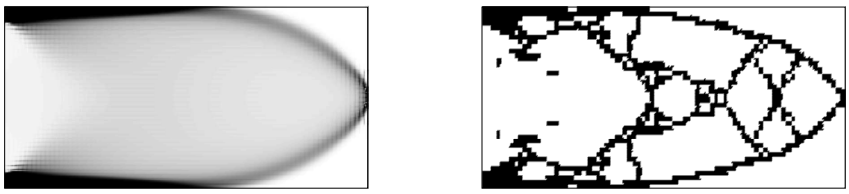

FIGURE 6. Plot of $\mathfrak{h}'_\delta$ with $\eta = 2 \cdot 10^{-2}$ and a 80×40 mesh. The regularization in the left figure is $\delta \approx 1.5 \cdot 10^{-3}$.

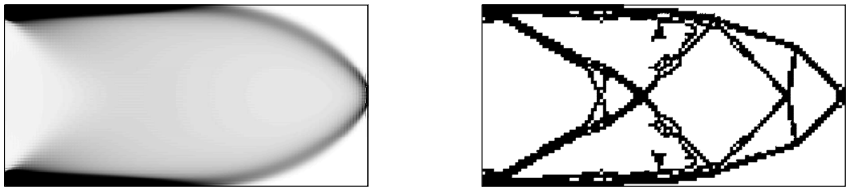

FIGURE 7. Plot of $\mathfrak{h}'_\delta$ with data as in Figure 6 but with a 240×120 mesh. The compliance of the discrete design is here $1.6 \cdot 10^{-2}$ compared with $3.6 \cdot 10^{-2}$ for the discrete design in Figure 6, and $9.7 \cdot 10^{-3}$ for the regularized designs.

iterations do not converge and we may need to restrict the amount of material allowed to change in each iteration. The right part of Figure 3 to Figure 7 shows the density after 100 iterations using a variant of (25) with $\delta = 0$ and with solutions from the left part of the figures taken as initial guesses. Here, ρ is updated elementwise and only a fraction of elements, corresponding to the smallest and largest values of v, is allowed to change, such that the volume remains constant. In all experiments, the compliance initially drops but eventually starts to oscillate, and at this point the control ρ will start to form checkerboard structures in large areas. To prevent the formation of such structures we here reduce the fraction of elements allowed to change as soon as the compliance starts to oscillate.

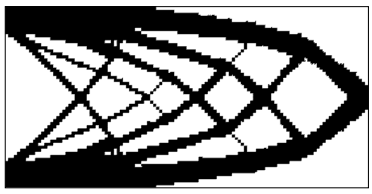

FIGURE 8. The relative material density when material has been iteratively removed from a completely filled domain by sorting $\varepsilon_{ij}(u)E_{ijkl}\varepsilon_{kl}(u)$ and removing the material corresponding to the largest values. In each iteration the volume to be removed is adjusted to follow a geometric sequence of volumes such that the final volume is the same as in Figure 4. The final compliance after 70 iterations has converged to $6.78 \cdot 10^{-3}$ compared to $6.65 \cdot 10^{-3}$ for the discrete iterations in Figure 4 and 5.

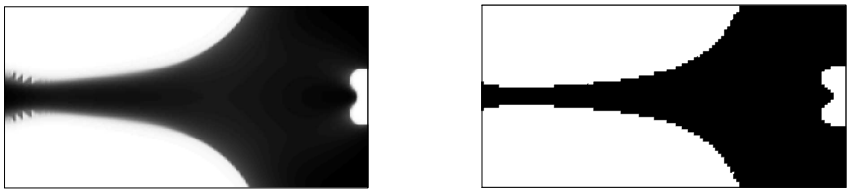

FIGURE 9. Plot of $\mathfrak{h}'_\delta$ as an approximation of the relative material density when maximizing compliance. A uniform mesh with 240×120 nine-node quadrilateral finite elements, a lower relative density $\rho_- = 0.5$, and a multiplier $\eta = 2 \cdot 10^{-3}$, was used. The discrete iterations give no further information in this case.

It can also be noted that the expression $\mathfrak{v} \equiv \eta - \varepsilon_{ij}(u)E_{ijkl}\varepsilon_{kl}(u)$ resembles the the topological gradient used in the topological shape method [4]. The topological

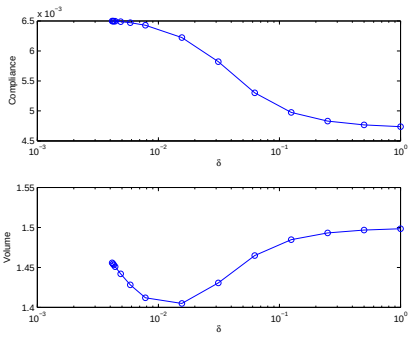

FIGURE 10. Convergence history for the compliance maximization problem. Although the volume does not converge as the regularization decreases, the compliance here seems to increase and level out. For comparison the compliance for a intuitive guess, with ρ_- close to the left and right boundary, ρ_+ in the middle, and the same volume, gives a compliance of $5.7 \cdot 10^{-3}$ compared with $6.4 \cdot 10^{-3}$ in the figure. Also, note that the Newton iterations fail to converge for small regularizations.

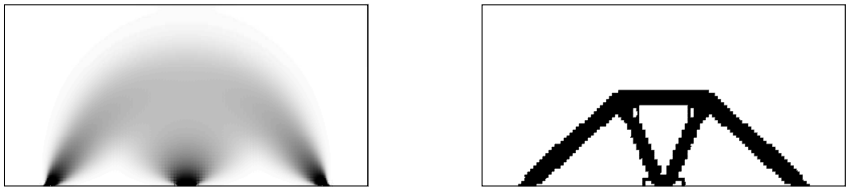

FIGURE 11. The compliance minimization problem for a downward force $f_s(x, 0) = -10$, $x \in [0.95, 1.05]$, and with supports located at $x \in [0.2, 0.25]$ and $x \in [1.75, 1.8]$. Both supports are fixed in both the x- and y-direction. A uniform mesh with 240×120 elements and a multiplier $\eta = 5 \cdot 10^{-3}$ was used. In the left plot the regularization is $\delta \approx 10^{-3}$ and the compliance is $1.3 \cdot 10^{-3}$. The compliance after 100 discrete iterations, shown in the right plot, is $1.5 \cdot 10^{-3}$.

shape method starts from a completely filled domain and successively removes material according to the sign of the topological derivative. This method is appealing since it is simple and gives interesting designs, but it may not converge to the true optimal design if it is possible to remove too much material, which never can be added again. In Figure 8, material has been iteratively removed from a completely filled domain by sorting $\varepsilon_{ij}(u)E_{ijkl}\varepsilon_{kl}(u)$ and removing the material corresponding to the largest values. In each iteration the volume to be removed is adjusted to follow a geometric sequence such that the final volume is approximately the same as the one in Figures 3 and 4.

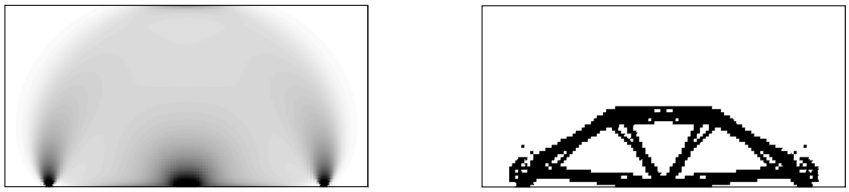

FIGURE 12. The compliance minimization problem with data as in Figure 11 but with both supports fixed in the y-direction and free to move in the x-direction. The smallest regularization was $\delta \approx 10^{-3}$ with a compliance of $1.5 \cdot 10^{-3}$. The compliance after 100 discrete iterations was $2.8 \cdot 10^{-3}$.

As a comparison with the concave maximization problem of minimizing compliance, it is interesting to see what happens for the problem of maximizing compliance. Replacing the 'inf' in (24) with a 'sup' gives, similarly to Section 3, a regularized Hamiltonian which only has a unique minimizer for sufficiently large regularizations. In Figure 9, the Pontryagin method is used to maximize compliance by placing two materials with $\rho \in \{0.5, 1\}$. The reason to not have $\rho_- = 10^{-3}$, is that maximizing compliance here seems to lead to a structure not connected to the part of the boundary where the external force is applied, thus making the problem harder to solve. It is also not clear that the solution for a small value of ρ_- is a good approximation of the solution for $\rho_- = 0$ in this example. The solution to the regularized Hamiltonian system gives, in Figure 9, a design which has the interesting shape of a turning fork. In Figure 10, we see that the Newton iterations do not converge for small regularizations, which indicates that there does not longer exist any minimizer to the regularized Hamiltonian. Also, discrete iterations with (25) does not give any additional information.

Finally, in Figures 11 and 12 the compliance minimization problem is solved for a slightly different example where a downward force is applied to the middle of the lower side, $f_s(x, 0) = -10$, $x \in [0.95, 1.05]$, and supports are located at $x \in [0.2, 0.25]$ and $x \in [1.75, 1.8]$. In Figure 11 the supports are fixed in both the x- and y-direction whereas they are only fixed in the y-direction in Figure 12.

4.2. **Interior Reconstruction.** For the compliance optimization problem (6) symmetry, $u = \lambda$, reduced the Hamiltonian system to the variational equation (23). Symmetry is common in many optimization problems connected to minimization of energy, but there are important exceptions such as inverse problems related to reconstruction from measurements. For example, consider the multi-experiment case of the reconstruction problem (8) stated in Section 1: reconstruct an unknown density $\rho : \Omega \to \{\rho_-, 1\}$ from M different boundary measurements $u_{meas,i}$, $i = 1, \dots, M$ on Γ_N resulting from applying given forces $f_{s,i}, f_{b,i} : \Gamma_N \to \mathbb{R}^d$, $i = 1, \dots, M$. One strategy is then to find the density ρ such that

$$\inf_{\rho:\Omega\to\{\rho_-,1\}} \Big\{ \sum_{m=1}^{M} \int_{\Gamma_N} |u_m - u_{meas,m}|^2 \, \mathrm{d}s \;\Big|\; a_\rho(u_m, v) = l_m(v),\ \forall v \in V,\ m = 1, \dots, M \Big\}, \tag{26}$$

where $a_\rho(u,v)$ is given by (2) and the compliance is given by

$$l_m(u) \equiv \int_\Omega f_{b,m} \cdot u \, \mathrm{d}x + \int_{\Gamma_N} f_{s,m} \cdot u \, \mathrm{d}s.$$

The Lagrangian is then

$$\mathcal{L}(u_1,\dots,u_M,\lambda_1,\dots,\lambda_M,\rho) = \sum_{m=1}^{M} \int_{\Gamma_N} |u_m - u_{meas,m}|^2 \, \mathrm{d}s + l_m(\lambda_m) + \int_\Omega \underbrace{-\rho \sum_{m=1}^{M} \varepsilon_{ij}(u_m) E_{ijkl} \varepsilon_{kl}(\lambda_m)}_{\mathfrak{v}} \, \mathrm{d}x,$$

and the Hamiltonian is

$$H = \sum_{m=1}^{M} \int_{\Gamma_N} |u_m - u_{meas,m}|^2 \, \mathrm{d}s + l_m(\lambda_m) + \int_\Omega \underbrace{\min_{\rho \in \{\rho_-,1\}} \{\rho \mathfrak{v}\}}_{\mathfrak{h}(\mathfrak{v})} \, \mathrm{d}x. \tag{27}$$

In this case no symmetry is present and the regularized Hamiltonian system becomes

$$\begin{aligned} a_{\mathfrak{h}'_\delta}(u_m, v_m) \, \mathrm{d}x &= l_m(v_m), \\ a_{\mathfrak{h}'_\delta}(u_m, w_m) \, \mathrm{d}x &= 2 \int_{\Gamma_N} (u_m - u_{meas,m}) \cdot w_m \, \mathrm{d}s, \end{aligned} \tag{28}$$

for all test functions $v_m, w_m \in V$, $m = 1,\dots,M$. Note, that replacing $\rho : \Omega \to \{\rho_-, 1\}$, in the original formulation (26), with $\rho : \Omega \to [\rho_-, 1]$, gives the same Hamiltonian (27).

FIGURE 13. Material densities to be reconstructed. The density is 0.5 in the white region, and 1 elsewhere.

In Figures 14 and 17 the system (28) is solved, for $M = 1, 2$, using the finite element method on a quadrilateral 40×40 mesh with nine-node elements, and Newton iterations. In all examples we use the computational domain $\Omega = (-1,1) \times (-1,1)$, with a fixed right boundary, and external boundary forces applied to the lower and left boundaries. Two sets of measurements were simulated by solving (4) on a quasi-uniform triangular mesh with 28000 quadratic Lagrange elements, for a given material density, with applied boundary forces $f_{s,1} = (10\cos(\pi y/2), 0)$ on the left boundary and $f_{s,2} = (0, 10\cos(\pi x/2))$ on the lower boundary. No external force is applied to the top boundary and no volume forces are present. In all examples we use $\rho : \Omega \to \{0.5, 1\}$ and seek to reconstruct two cases of material distributions:

FIGURE 14. Approximated material density, $\mathfrak{h}'_\delta$, from reconstruction of the amoeba shaped density. Left: Measurements from one experiment. Right: Measurements from two experiments. Using measurements from two different experiments here sharpens the edges and better resolves the region close to the fixed boundary.

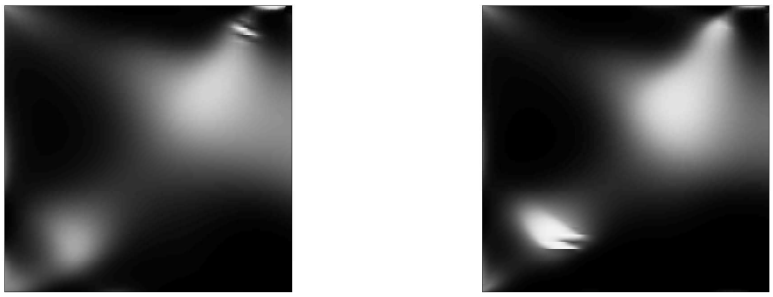

FIGURE 15. Material density reconstructed from experiment with an amoeba and a circle. Left: Data from one experiment is used. Right: Data from two experiments is used. In this example the reconstructed density does not gain much from using multiple measurements. Choosing different boundary forces could here potentially give an improvement of the finest details of the amoeba shape.

First we use a material with a density distribution in the form of an amoeba (see left part of Figure 13),

$$\rho = \begin{cases} 1, & x^2 + (y-0.1)^2 \geq 0.2 + 0.1e^{1.4\cos(3\theta-2)+0.4\sin^2\theta} \\ 0.5, & x^2 + (y-0.1)^2 < 0.2 + 0.1e^{1.4\cos(3\theta-2)+0.4\sin^2\theta} \end{cases}$$

with $\theta = \arctan(x/(y-0.1))$. Then, we combine the amoeba shape with a circle of radius 0.2, see right part of Figure 13.

In figure 14 and 15, we see how using multiple experiments increases the quality of the recovered material distribution, and in Figure 16 we see how the quality decreases after adding Gaussian random values to the measured data. The added noise is here scaled to correspond to 5% of the measured data. Note that despite the bad reconstructions in Figure 16, the $L^2(\partial\Omega)$ error between u and the noisy measurements u_{meas} levels out, so we can in this case therefore not hope for a better

reconstruction, even if we continue to reduce the regularization. This is known as the discrepancy principle, see [6] and [13].

As in section 4.1, discrete iterations in ρ and u can be done as post-processing to remove intermediate values of ρ. Such iterations does not, however, seem to give any additional information in this example. Also, using a small value for ρ_- to mimic void, makes the problem too ill-posed to solve with such accuracy in the reconstructed density as in the examples shown here. From our experience, solving the system (28) for a small ρ_- only seems possible for reconstruction of small circular inclusions close to the boundaries.

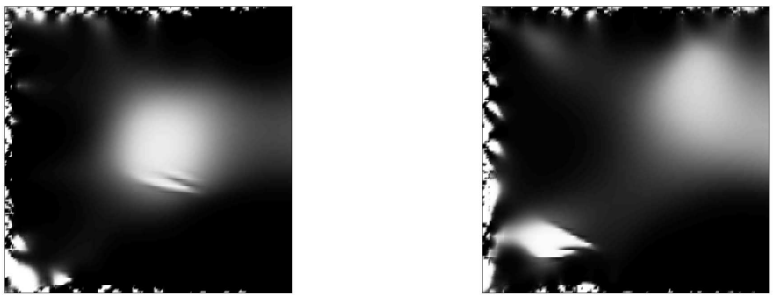

FIGURE 16. Material density reconstructed from noisy data, using two experiments and adding 5% white noise to the measured data. Although, artifacts are here introduced near the forced boundaries, and the resolution of the shapes is lost, the positions of the regions are still visible.

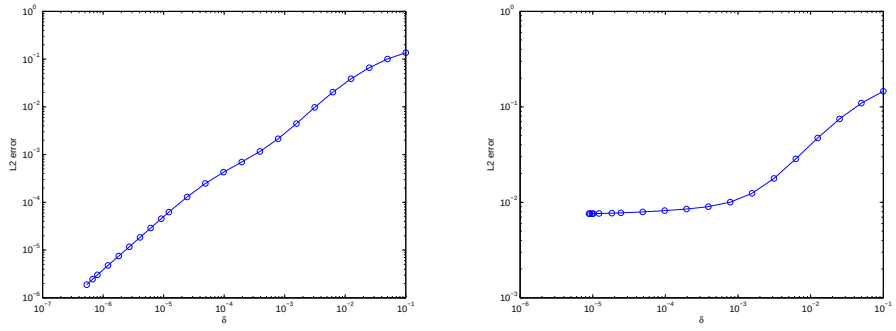

FIGURE 17. Plot of the $L^2(\partial\Omega)$ norm of $u - u_{meas}$ with respect to the regularization. Left: Error history corresponding to the single experiment case in Figure 14. Right: Error history corresponding to the single experiment case in Figure 15. The error in the right figure reaches its minimum value, and no better reconstruction can here be expected without additional post-processing of the measurements.

References

[1] Grégoire Allaire. *Shape optimization by the homogenization method*, volume 146 of *Applied Mathematical Sciences*. Springer-Verlag, Nw York, 2002.

[2] M. P. Bendsøe and O. Sigmund. *Topology optimization*. Springer-Verlag, Berlin, 2003. Theory, methods and applications.

[3] Jesper Carlsson, Mattias Sandberg, and Anders Szepessy. Symplectic Pontryagin approximations for optimal design. *preprint*, 2006.

[4] Jean Céa, Stéphane Garreau, Philippe Guillaume, and Mohamed Masmoudi. The shape and topological optimizations connection. *Comput. Methods Appl. Mech. Engrg.*, 188(4):713–726, 2000. IV WCCM, Part II (Buenos Aires, 1998).

[5] Bernard Dacorogna. *Direct methods in the calculus of variations*, volume 78 of *Applied Mathematical Sciences*. Springer-Verlag, Berlin, 1989.

[6] Heinz W. Engl, Martin Hanke, and Andreas Neubauer. *Regularization of inverse problems*, volume 375 of *Mathematics and its Applications*. Kluwer Academic Publishers Group, Dordrecht, 1996.

[7] Robert V. Kohn and Gilbert Strang. Optimal design and relaxation of variational problems. I. *Comm. Pure Appl. Math.*, 39(1):113–137, 1986.

[8] Robert V. Kohn and Gilbert Strang. Optimal design and relaxation of variational problems. II. *Comm. Pure Appl. Math.*, 39(2):139–182, 1986.

[9] Robert V. Kohn and Gilbert Strang. Optimal design and relaxation of variational problems. III. *Comm. Pure Appl. Math.*, 39(3):353–377, 1986.

[10] Olivier Pironneau. *Optimal shape design for elliptic systems*. Springer Series in Computational Physics. Springer-Verlag, New York, 1984.

[11] M. Sandberg and A. Szepessy. Convergence rates of symplectic Pontryagin approximations in optimal control theory. *M2AN*, 40(1), 2006.

[12] Mattias Sandberg. Convergence rates for numerical approximations of an optimally controlled Ginzburg-Landau equation. *preprint*, 2006.

[13] Curtis R. Vogel. *Computational methods for inverse problems*, volume 23 of *Frontiers in Applied Mathematics*. Society for Industrial and Applied Mathematics (SIAM), Philadelphia, PA, 2002. With a foreword by H. T. Banks.

Department of Numerical Analysis, Royal Institute of Technology, 100 44, Sweden
E-mail address: jesperc@nada.kth.se
URL: nada.kth.se/~jesperc